

# Surface embedding narrow volume reconstruction from unorganized points <sup>☆</sup>



Yibao Li <sup>a</sup>, Dongsun Lee <sup>b</sup>, Chaeyoung Lee <sup>b</sup>, Jihu Lee <sup>c</sup>, Sanha Lee <sup>c</sup>, Jisu Kim <sup>c</sup>, Shinwoo Ahn <sup>c</sup>, Junseok Kim <sup>b,\*</sup>

<sup>a</sup> Department of Computational Science and Engineering, Yonsei University, Seoul 120-749, Republic of Korea

<sup>b</sup> Department of Mathematics, Korea University, Seoul 136-713, Republic of Korea

<sup>c</sup> Seoul Science High School, Seoul 110-530, Republic of Korea

## ARTICLE INFO

### Article history:

Received 10 January 2013

Accepted 4 February 2014

Available online 13 February 2014

### Keywords:

Volume reconstruction

Allen–Cahn equation

Unsigned distance function

Multigrid method

Unconditional stability

## ABSTRACT

In this paper, we present a novel fast and accurate numerical method for the surface embedding narrow volume reconstruction from unorganized points in  $\mathbb{R}^3$ . Though the level set method prevails in the image processing, it requires a redistancing procedure to maintain a desired shape of the level set function. On the other hand, our method is based on the Allen–Cahn equation, which has been applied in image segmentation due to its motion by mean curvature property. We modify the original Allen–Cahn equation by multiplying a control function to restrict the evolution within a narrow band around the given surface data set. To improve the numerical stability of our proposed model, we split the governing equation into linear and nonlinear terms and use an operator splitting technique. The linear equation is solved by the multigrid method which is a fast solver and the nonlinear equation is solved analytically. The unconditional stability of the proposed scheme is also proved. Various numerical results are presented to demonstrate the robustness and accuracy of the proposed method.

© 2014 Elsevier Inc. All rights reserved.

## 1. Introduction

The industry of rapid prototyping and 3D printing has emerged in past years, and the 3D printing technology to visualize objects in space is now one of the issues in mathematics [1] and computer science [2]. This work has been motivated by the need for 3D printing [3,4] from surface data. The basic mechanism of the 3D printer is that it builds up the object layer by layer. However, a surface is two-dimensional (see Fig. 1(a)) and its slices are in general one-dimensional, which 3D printer cannot build up a three-dimensional object. Hence, to print the surface with a 3D printer, we need to thicken up the surface and make a surface embedding narrow volume (Fig. 1(b)). Fig. 1(c) shows a physical model manufactured from the proposing mathematical model. Even though we were motivated by 3D surface printing, our proposing algorithm is general so that the algorithm can be applied to other applications such as geometry processing [5], tolerance analysis in machine processing [6], and collision detection [7,8].

Up to now, a great number of algorithms have been proposed to solve the offset surface reconstruction problems. In [9], Liu and Wang approximated both the zero-level surface and its offset surface using an implicit function. They also developed a fast offset surface generation method via a narrow band signed distance-field [10]. In addition, Chen and Wang proposed thickening operations to convert a surface to a solid [11] and introduced a uniform offsetting model [12]. It enables to generate both grown and shrunk models from arbitrary offset distance. Curless and Levoy developed two important techniques for reconstructing complex and accurate models from scanned objects: spacetime analysis,  $d$  based on analyzing the time evolution of the structured light reflections [13], and a volumetric space carving technique for integrating several data into a single geometric model [14]. Lien [15] and Varadhan and Manocha [16] demonstrated representations of the Minkowski sum boundary. To get high-quality offsets, an adaptive octree-structure was used for distance bounds in [17]. Small and thin features were detected by subdivisional methods [18,19]. For some other considerations of offset surface reconstruction, we also refer to [20,21]. Recently, Wang and Manocha [22] presented a highly parallel method to compute the approximate offsetting on models represented by structured points in layered depth images (LDIs). The main idea is to compute the super-union of all the balls

<sup>☆</sup> This paper has been recommended for acceptance by Carlo Colombo, Ph.D.

\* Corresponding author.

E-mail address: [cfdkim@korea.ac.kr](mailto:cfdkim@korea.ac.kr) (J. Kim).

URL: <http://www.math.korea.ac.kr/~cfdkim> (J. Kim).

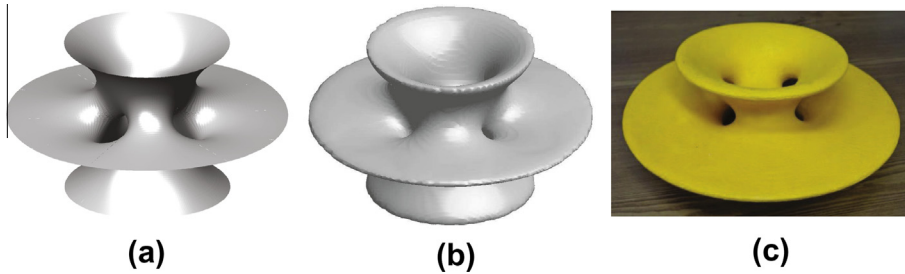


Fig. 1. (a) Surface, (b) reconstructed volume, and (c) a physical model manufactured from the proposing mathematical model.

centered at the sample points, which can be conducted efficiently on the graphics processing unit with LDI representation. As compared to prior CPU-based approximation offsetting algorithms, their approach results in more than 100 times speedups.

Our approach is basically an implicit representation of interface as an isosurface of the level set function [23–25]. The level set method for numerical interface evolution has been successfully used for surface reconstruction, including texture objects [26–31]. Zhao et al. solved shape reconstruction problems by using a minimal-surface-like model and the level set method [30,31]. However, for offset surface reconstruction problem, the calculation of unsigned distance function is a challenging problem because the offset distance is generally small and the given surface is not closed. To solve these problems, we present a novel fast and accurate numerical method for surface embedding narrow volume reconstruction from an unorganized surface data set. Our method is based on the Allen–Cahn (AC) equation [32], which has been applied to image processing problems such as segmentation, denoising, and inpainting [33–39]. We choose the AC equation because it has intrinsic smoothing effect on interfacial transition layers and its fast and accurate hybrid numerical solver is available [40]. We modify the original AC equation by multiplying a control function to restrict the evolution within a narrow band around the given surface data set. The stability of numerical schemes for equations is very important. Explicit time integration schemes are generally only conditionally stable and require small time steps to insure numerical stability. Using an operator splitting technique, we propose the scheme that allows the use of a sufficiently large time step without the technical limitations. We also prove the unconditional stability of the proposed scheme.

This paper is organized as follows. In Section 2, we briefly describe the main governing equation and we describe the numerical solution and prove its unconditional stability. In Section 3, we perform some characteristic numerical experiments for volume reconstruction. Finally, our conclusion is given in Section 4.

## 2. Proposed method and numerical solution

### 2.1. Proposed method

For a given set of unorganized surface data points  $S = \{\mathbf{X}_m = (X_m, Y_m, Z_m) \in \mathbb{R}^3 | m = 1, \dots, M\}$ , we want to reconstruct a narrow volume which embeds  $S$ . Here we mean by a volume the enclosed volume by the isosurface of a scalar-valued function. Without loss of generality we can assume  $S \subset \Omega = (0, L_x) \times (0, L_y) \times (0, L_z)$ . Let  $h = L_x/N_x = L_y/N_y = L_z/N_z$  be the uniform grid size and  $\Omega_h = \{\mathbf{x}_{ijk} = (x_i, y_j, z_k) | x_i = (i - 0.5)h, y_j = (j - 0.5)h, z_k = (k - 0.5)h, 1 \leq i \leq N_x, 1 \leq j \leq N_y, 1 \leq k \leq N_z\}$  be the set of cell centers, where  $N_x, N_y$ , and  $N_z$  are power of two.

A simplest method for the volume reconstruction is to find an unsigned distance function from  $S$ , and then we define the volume bounded by the isosurface of the function at an order of  $h$  value. For

better visualization, let us consider the simplest method in two-dimensional space. Fig. 2(a) shows  $S$ . Include  $S$  by a domain  $\Omega$  and discretize the domain with  $\Omega_h$  (open circles in Fig. 2(b)). Then define the unsigned discrete distance function on  $\Omega_h$  as

$$d(\mathbf{x}_{ijk}) = \min_{1 \leq m \leq M} |\mathbf{x}_{ijk} - \mathbf{X}_m|. \quad (1)$$

In Fig. 2(b), the dash-dot line segment is  $|\mathbf{x}_{ijk} - \mathbf{X}_m|$ . Fig. 2(c) shows the mesh plot of the unsigned distance function. However the isosurface of Eq. (1) is generally not smooth as shown in Fig. 2(d).

To overcome this non-smoothness of the isosurface and get a smooth narrow volume embedding unorganized point data set, we propose the following modified Allen–Cahn model with Neumann boundary condition:

$$\frac{\partial \phi(\mathbf{x}, t)}{\partial t} = g(\mathbf{x}) \left( -\frac{F'(\phi(\mathbf{x}, t))}{\epsilon^2} + \Delta \phi(\mathbf{x}, t) \right) \text{ in } \Omega, \quad (2)$$

$$\mathbf{n} \cdot \nabla \phi(\mathbf{x}, t) = 0 \text{ on } \partial \Omega, \quad (3)$$

where  $F(\phi) = 0.25(1 - \phi^2)^2$ ,  $\epsilon$  is a positive constant, and  $\mathbf{n}$  is the outward normal vector at the domain boundary. If  $g(\mathbf{x}) \equiv 1$ , then Eq. (2) is the classical AC equation, which was proposed to model the motion of antiphase domain coarsening in a binary alloy and was applied to segmentation, denoising and inpainting [33–39] due to its motion by mean curvature.  $\phi$  is called as a phase field. In our approach, we define the initial profile as

$$\phi(\mathbf{x}, 0) = \tanh \left( \frac{l - d(\mathbf{x})}{\sqrt{2}\xi} \right). \quad (4)$$

Here  $l$  is the offset distance and  $\xi$  is related to the interface transition thickness. We choose  $\xi$  smaller than  $\epsilon$ , which means the initial profile has sharper interfacial transition than locally well-relaxed interfacial profiles. Then using Eq. (4), we define the non-constant function,  $g(\mathbf{x})$ :

$$g(\mathbf{x}) = 1 - \phi^2(\mathbf{x}, 0), \quad (5)$$

which restricts the evolution of the governing Eq. (2) within a narrow band around the given surface data set. Let us take a two-dimensional example. Assume that we are given point data of a circle with a radius 0.25. Then, Fig. 3(a)–(c) show the unsigned distance function  $d(x, y) = \left| \sqrt{x^2 + y^2} - 0.25 \right|$ , the initial order parameter  $\phi(x, y, 0)$ , and  $g(x, y)$ , respectively. Fig. 3(d) shows the slice plots of  $d(x, 0.5)$ ,  $\phi(x, 0.5, 0)$ , and  $g(x, 0.5)$  at  $y = 0.5$ . The function  $g(x, y)$  is positive on the transition layers of  $\phi(x, y, 0)$  and zero elsewhere.

### 2.2. Numerical solution

Next, we present an operator splitting-based hybrid numerical scheme for Eq. (2) in a three-dimensional domain  $\Omega = (0, L_x) \times (0, L_y) \times (0, L_z)$ . Let  $\phi_{ijk}^n$  be approximations of  $\phi(x_i, y_j, z_k, n\Delta t)$ , where  $\Delta t = T/N_t$  is the time step,  $T$  is the final time,

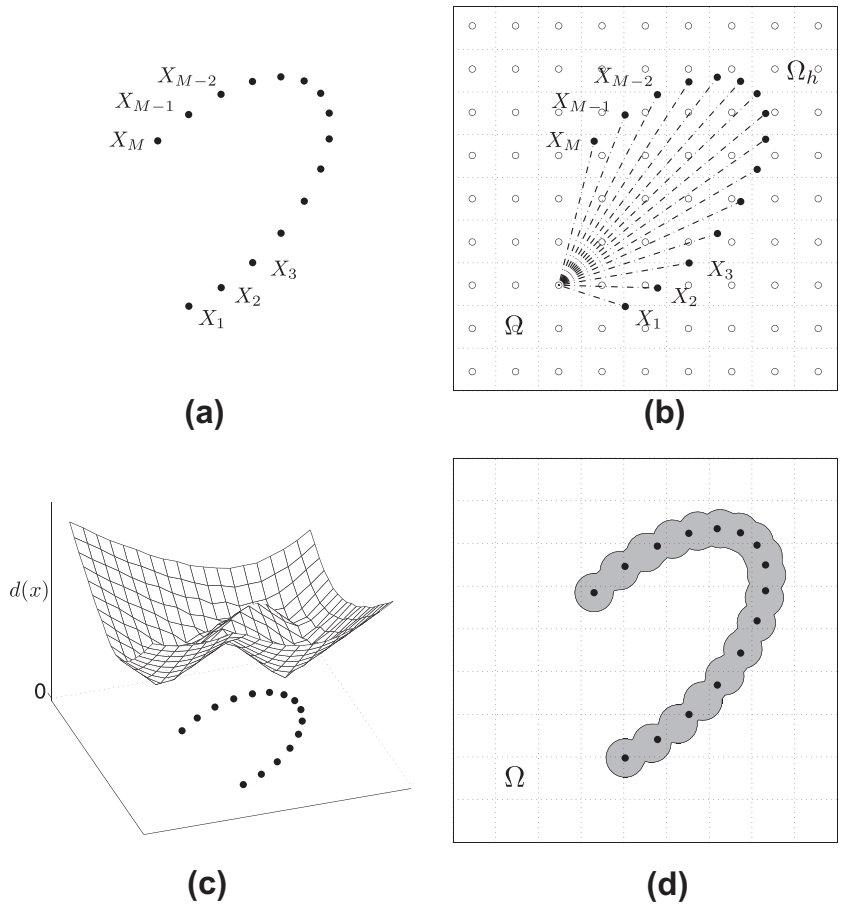


Fig. 2. (a) Schematic illustration of data set  $S$ , (b) definition of unsigned discrete distance function, (c) mesh plot of unsigned distance function, and (d) contouring a level of distance function.

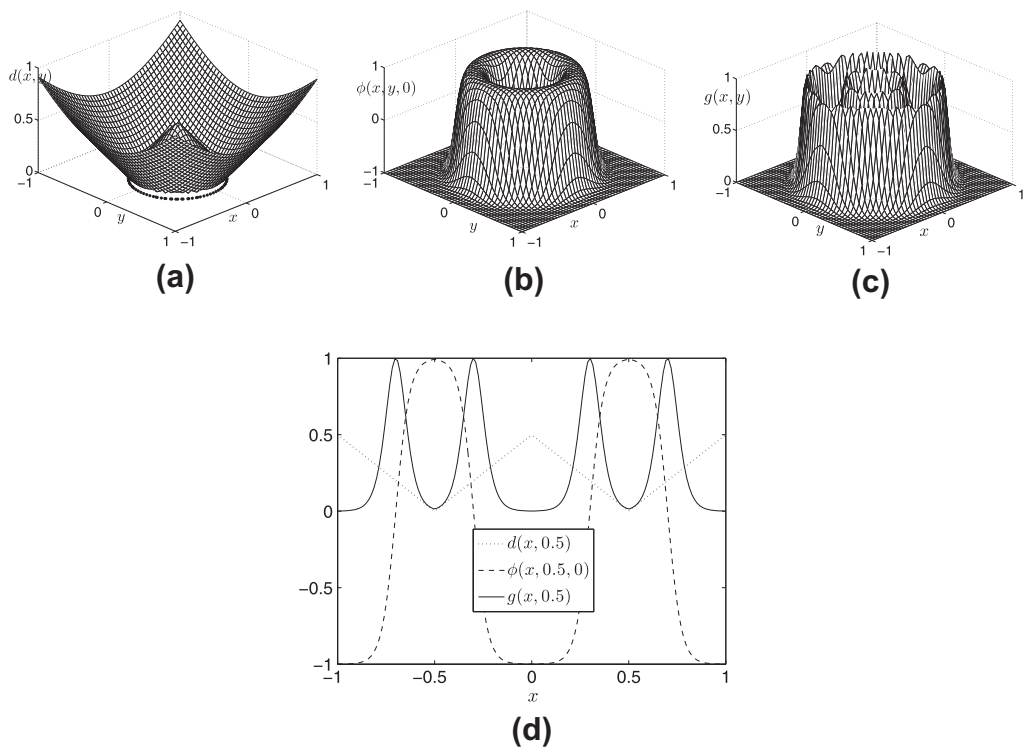


Fig. 3. (a)–(c) are the unsigned distance function  $d(x,y) = |\sqrt{x^2 + y^2} - 0.25|$ , the initial order parameter  $\phi(x,y,0)$ , and  $g(x,y)$ , respectively. (d) the slice plots of  $d(x,0.5)$ ,  $\phi(x,0.5,0)$ , and  $g(x,0.5)$  at  $y=0.5$ .

and  $N_t$  is the total number of time steps. We split the original problem (2) into a sequence of simpler problems as

$$\frac{\partial \phi(\mathbf{x}, t)}{\partial t} = \mathbf{g}(\mathbf{x}) \Delta \phi(\mathbf{x}, t), \tag{6}$$

$$\frac{\partial \phi(\mathbf{x}, t)}{\partial t} = -\frac{\mathbf{g}(\mathbf{x}) F'(\phi(\mathbf{x}, t))}{\epsilon^2}. \tag{7}$$

As the first step, we solve Eq. (6) by applying an implicit method with  $\phi^n$  and homogeneous Neumann boundary condition, that is,

$$\begin{aligned} \frac{\phi_{ijk}^{n+\frac{1}{2}} - \phi_{ijk}^n}{\Delta t} &= \mathbf{g}_{ijk} \Delta_d \phi_{ijk}^{n+\frac{1}{2}} \\ &= \frac{\mathbf{g}_{ijk}}{h^2} \left( \phi_{i-1,j,k}^{n+\frac{1}{2}} + \phi_{i+1,j,k}^{n+\frac{1}{2}} + \phi_{i,j-1,k}^{n+\frac{1}{2}} + \phi_{i,j+1,k}^{n+\frac{1}{2}} + \phi_{i,j,k-1}^{n+\frac{1}{2}} + \phi_{i,j,k+1}^{n+\frac{1}{2}} \right. \\ &\quad \left. - 6\phi_{ijk}^{n+\frac{1}{2}} \right). \end{aligned} \tag{8}$$

The linear system of Eq. (8) is solved using a multigrid method [41], specifically, V-cycles using the Gauss–Seidel relaxation with a tolerance  $1e-7$ . The Gauss–Seidel iteration for Eq. (8) is given as

$$\begin{aligned} \phi_{ijk}^{n+\frac{1}{2},m+1} &= \left[ \phi_{ijk}^n + \frac{\Delta t \mathbf{g}_{ijk}}{h^2} \left( \phi_{i-1,j,k}^{n+\frac{1}{2},m+1} + \phi_{i+1,j,k}^{n+\frac{1}{2},m} + \phi_{i,j-1,k}^{n+\frac{1}{2},m+1} + \phi_{i,j+1,k}^{n+\frac{1}{2},m} \right. \right. \\ &\quad \left. \left. + \phi_{i,j,k-1}^{n+\frac{1}{2},m+1} + \phi_{i,j,k+1}^{n+\frac{1}{2},m} \right) \right] / \left( 1 + \frac{6\Delta t \mathbf{g}_{ijk}}{h^2} \right), \end{aligned} \tag{9}$$

where  $m + 1$  denotes the new approximation and  $m$  the old approximation of the iteration. In the coarse grid,  $\mathbf{g}_{ijk}$  is evaluated using the average of the closest eight neighborhood points  $\phi_{ijk}^0$  value. For example, in  $\Omega_{2h}$  grid,

$$\begin{aligned} \mathbf{g}_{ijk} &= 1 - \left( \phi_{2i,2j,2k}^0 + \phi_{2i-1,2j,2k}^0 + \phi_{2i,2j-1,2k}^0 + \phi_{2i-1,2j-1,2k}^0 + \phi_{2i,2j,2k-1}^0 \right. \\ &\quad \left. + \phi_{2i-1,2j,2k-1}^0 + \phi_{2i,2j-1,2k-1}^0 + \phi_{2i-1,2j-1,2k-1}^0 \right)^2 / 64 \end{aligned}$$

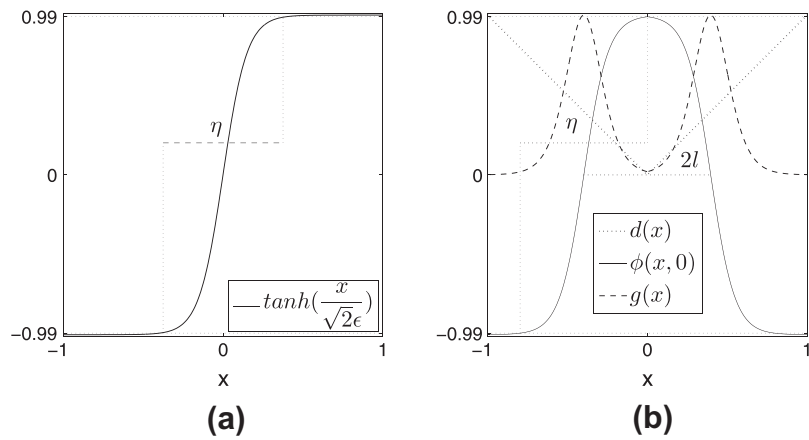


Fig. 4. (a) Equilibrium phase field profile,  $\tanh(x/(\sqrt{2}\epsilon))$ . (b) For a point data at the origin,  $d(x)$ ,  $\phi(x,0)$ , and  $g(x)$ . Here we used  $\epsilon = 0.1$ .

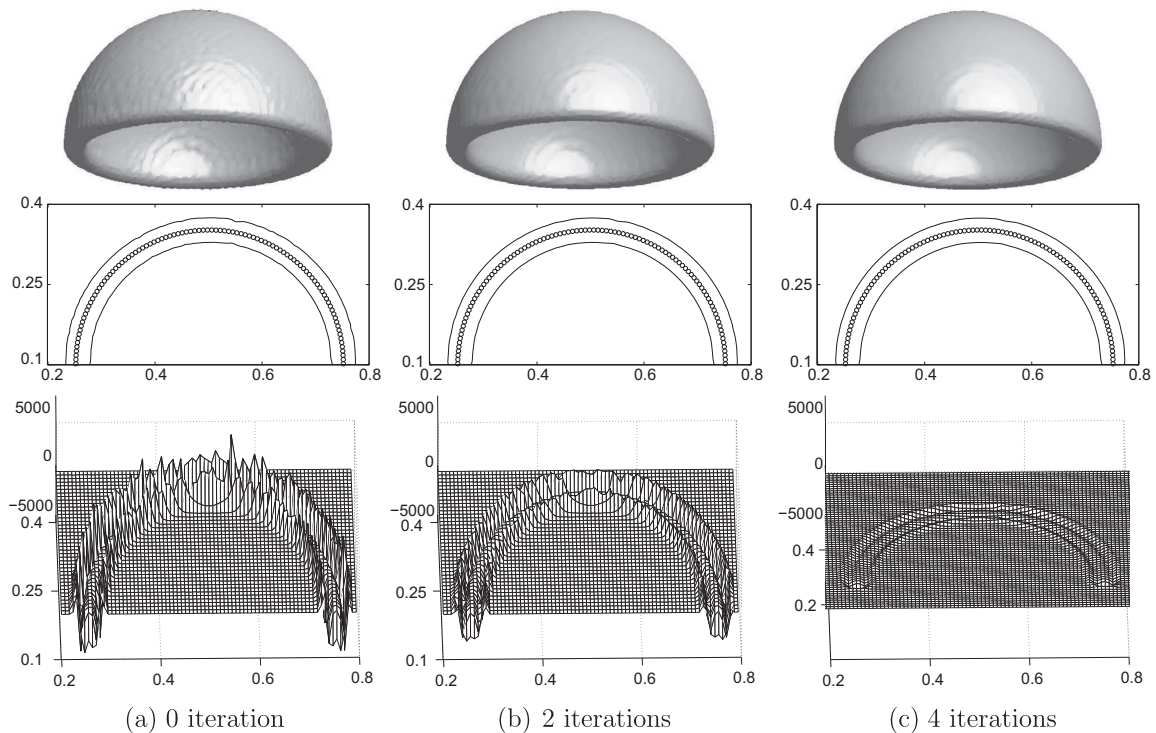


Fig. 5. Top row: the evolution of zero level set of  $\phi$ . Middle row: zero contours of  $\phi$  at the  $y = 0.5$  plane with surface data set (circles). Bottom row:  $-gF'(\phi)/\epsilon^2 + g\Delta\phi$  at the  $y = 0.5$  plane.

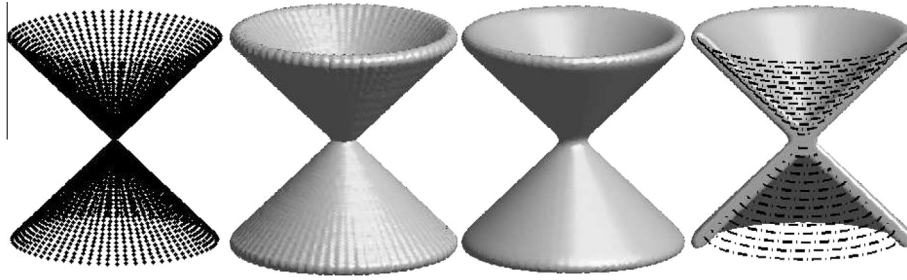


Fig. 6. From left to right: conical surface with 4270 data set points, initial reconstruction, final reconstruction, and cut off view of final reconstruction with data points.

for  $i = 1, \dots, N_x/2, j = 1, \dots, N_y/2,$  and  $k = 1, \dots, N_z/2$ . The rest of the multigrid algorithm is standard [41].

Next, for fixed  $\mathbf{x}$ , Eq. (7) is a separable ordinary differential equation [42], i.e.,

$$\frac{g}{\epsilon^2} dt + \frac{1}{\phi^3 - \phi} d\phi = 0. \quad (10)$$

If we solve Eq. (10) with the initial condition  $\phi_{ijk}^{n+\frac{1}{2}}$ , then we have the following solution after  $\Delta t$ :

$$\phi_{ijk}^{n+1} = \frac{\phi_{ijk}^{n+\frac{1}{2}}}{\sqrt{e^{\frac{2g_{ijk}\Delta t}{\epsilon^2}} + \left(\phi_{ijk}^{n+\frac{1}{2}}\right)^2 \left(1 - e^{\frac{2g_{ijk}\Delta t}{\epsilon^2}}\right)}}. \quad (11)$$

For more details about the numerical solution algorithm, see [40] in the case of  $g(\mathbf{x}) \equiv 1$ .

### 2.3. Stability of the proposed method

Our proposed hybrid splitting method, Eqs. (8) and (11), is an unconditionally stable scheme. First to prove the stability of Eq. (8), we consider the von Neumann analysis. We substitute  $\phi_{ijk}^n = \delta^n e^{\tau(\alpha i + \beta j + \gamma k)h}$  and  $\phi_{ijk}^{n+1/2} = \delta^{n+1/2} e^{\tau(\alpha i + \beta j + \gamma k)h}$  into Eq. (8). Here  $\delta, \alpha, \beta, \gamma$  are real parameters and  $\tau = \sqrt{-1}$ . Eq. (8) is a homogeneous heat equation with the variable coefficients  $g(\mathbf{x})$ . We can take an arbitrary point  $\hat{g}$  in the domain of Eq. (8) and freeze the coefficients at this point. Thus if the constant-coefficient heat equation satisfies the von Neumann spectral stability condition, the original Eq. (8) will be stable [43]. By substituting these terms into Eq. (8), we obtain

$$\delta = \frac{1}{1 + 4\hat{g}\Delta t \left( \sin^2(\alpha/2) + \sin^2(\beta/2) + \sin^2(\gamma/2) \right)}. \quad (12)$$

Since  $g(\mathbf{x})$  is nonnegative, the arbitrary point  $\hat{g}$  is nonnegative. Thus, from Eq. (12)  $\delta$  satisfies the property  $|\delta| \leq 1$  for any  $\alpha, \beta,$  and  $\gamma$ . Hence the numerical scheme of the constant-coefficient heat equation is unconditionally stable and Eq. (8) also holds it. Furthermore, the inequality  $\min_{ijk} \left( \phi_{ijk}^n \right) \leq \phi_{ijk}^{n+\frac{1}{2}} \leq \max_{ijk} \left( \phi_{ijk}^n \right)$  is satisfied by the discrete minimum and maximum principles for the heat equation [44]. Assume  $|\phi^n| \leq 1$ , we get  $|\phi^{n+\frac{1}{2}}| \leq 1$ . Second, for Eq. (11), it is obvious that  $\phi^{n+1} = 0$ , if  $\phi^{n+\frac{1}{2}} = 0$ . Otherwise we get

$$|\phi^{n+1}| = \frac{|\phi^{n+\frac{1}{2}}|}{\sqrt{e^{\frac{-2g\Delta t}{\epsilon^2}} + \left(\phi^{n+\frac{1}{2}}\right)^2 \left(1 - e^{\frac{-2g\Delta t}{\epsilon^2}}\right)}} = \frac{1}{\sqrt{1 + \left(\frac{1}{\left(\phi^{n+\frac{1}{2}}\right)^2} - 1\right) e^{\frac{-2g\Delta t}{\epsilon^2}}}} \leq 1.$$

Therefore, if  $|\phi^n| \leq 1$ , then  $|\phi^{n+1}| \leq 1$ . Hence our proposed scheme, Eqs. (8) and (11), is unconditionally stable for any time step.

### 3. Numerical results

In this section, we present numerical results using the proposed numerical algorithm on various synthetic and real data sets. For a good initial guess, let us consider one-dimensional space. For an equilibrium phase field profile,  $\tanh\left(x/(\sqrt{2}\epsilon)\right)$ , for Eq. (2), the phase field varies from  $-0.99$  to  $0.99$  over a distance of approximately  $\eta = 2\sqrt{2}\epsilon \tanh^{-1}(0.99)$  (refer to Fig. 4(a)). Therefore, if we want this value to be approximately  $m$  grid points, the  $\epsilon$  value needs to be taken as  $\epsilon_m = mh / [2\sqrt{2}\tanh^{-1}(0.99)]$  [45]. The offset distance  $l$  should be set as  $l \geq \eta/2$  to make  $g(x) > 0$  in the  $l$  offset region from the surface (Fig. 4(b)). Unless otherwise specified, throughout this paper we will use  $\xi = \epsilon_4$  and

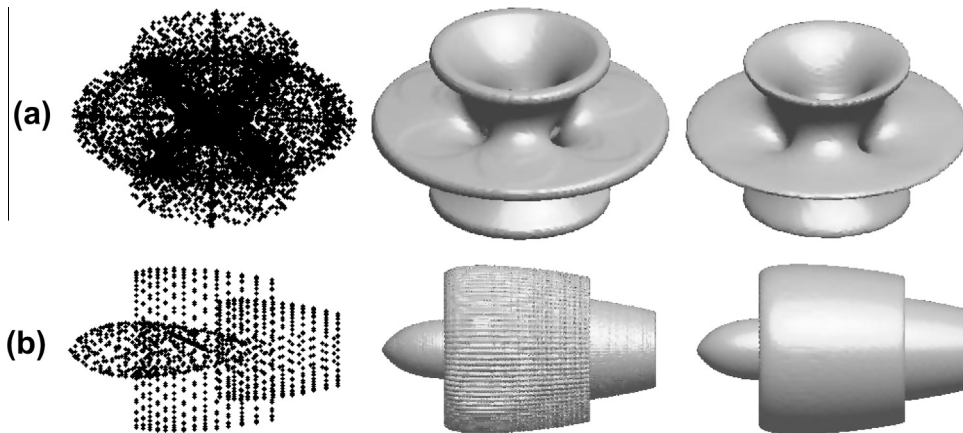


Fig. 7. Reconstructions of (a) Costa–Hoffman–Meeks and (b) engine surfaces. From left to right is surface data set, initial reconstruction, and final reconstruction, respectively.

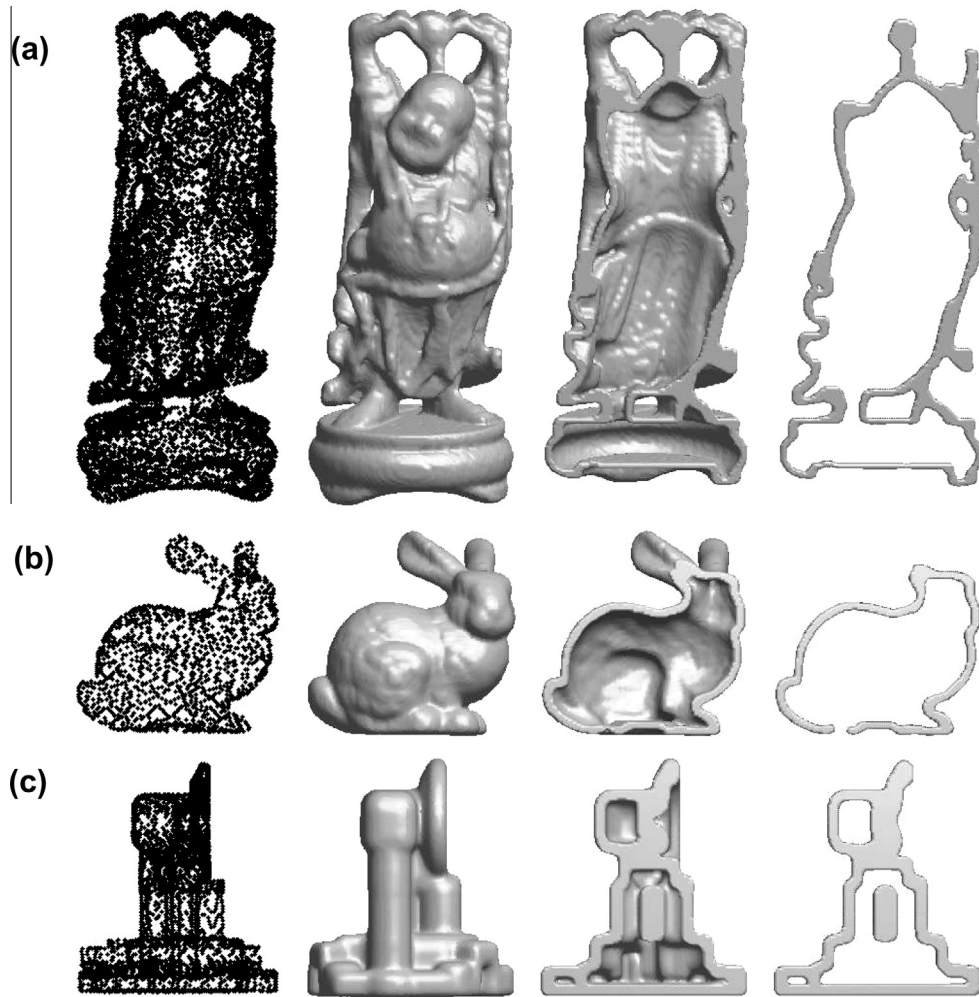


Fig. 8. Reconstructions of (a) happy Buddha, (b) bunny, and (c) oil pump. From left to right: initial reconstruction, final reconstruction, cut view, and cross view.

$l = \sqrt{2}\epsilon_5 \tanh^{-1}(0.99)$ . We also use  $\epsilon = \epsilon_{12}$  to get smooth offset surface and take the time step  $\Delta t = 5e - 5$ . For better visualization purposes, the points in some figures are displayed more sparsely than the real density.

We start with an example, which shows the basic mechanism of the algorithm, Eqs. (8) and (11). Let us consider a half sphere whose center is placed at  $(0.5, 0.5, 0.1)$  on the domain  $\Omega = (0, 1) \times (0, 1) \times (0, 0.5)$  and has a radius 0.25. The computation is run up to four iterations with  $128 \times 128 \times 64$  grid points. In the top row of Fig. 5, we show the evolution of zero level set of  $\phi$ . Columns (a)–(c) are at initial, two iterations, and four iterations, respectively. In the middle row we show the zero contours of  $\phi$  in the  $y = 0.5$  plane. To compare with the data set (circles), we put them together. As can be seen, offset distance is uniform along the curve of data set. Bottom row shows the right term in Eq. (2), i.e.,  $-gF'(\phi)/\epsilon^2 + g\Delta\phi$  in the  $y = 0.5$  plane. From the results in Fig. 5(c), we observe that the positive and negative values of the right term in Eq. (2) imply that  $\phi$  increases and decreases until the interface becomes smooth.

Fig. 6 shows the reconstruction of two headed cone whose input data size is 4270. From left to right, they are input data set, initial reconstruction, final reconstruction, and the comparison with initial data set, respectively. The computation takes eight iterations on the domain  $\Omega = (0, 1) \times (0, 1) \times (0, 1)$  with  $128 \times 128 \times 128$  grid points. As can be seen, our method achieves the reconstruction very fast. Comparison with the input data shows the uniform surface embedding volume.

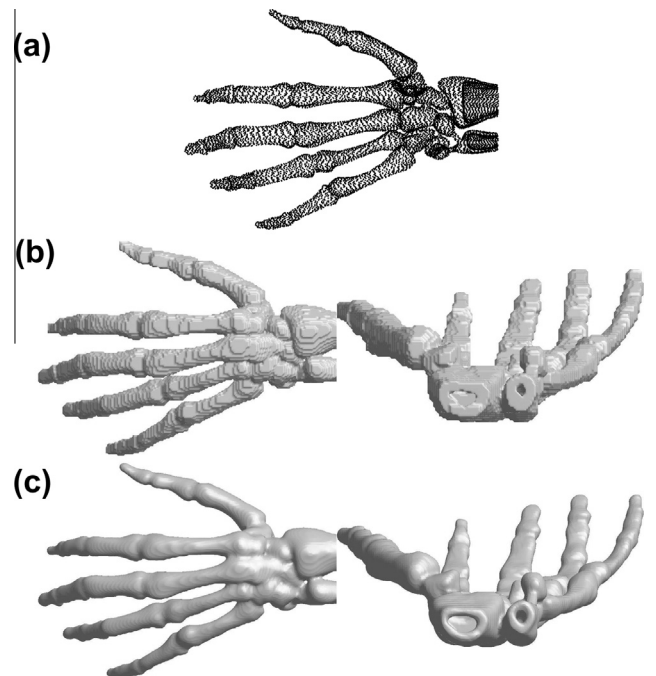


Fig. 9. Reconstruction of a skeleton hand. (a) initial data, (b) isosurface of distance function, and (c) final reconstruction.

**Table 1**  
List of data information and CPU times.

Case	Data points	Grid size	Iterations	CPU (s)
Fig. 5	2476	$128 \times 128 \times 64$	4	5.81
Fig. 6	4270	$128 \times 128 \times 128$	8	25.81
Fig. 7(a)	92,239	$128 \times 128 \times 128$	10	30.02
Fig. 7(b)	22,886	$256 \times 128 \times 128$	6	41.82
Fig. 8(a)	271,826	$128 \times 128 \times 256$	7	50.71
Fig. 8(b)	17,974	$256 \times 256 \times 256$	6	167.32
Fig. 8(c)	30,937	$128 \times 128 \times 128$	6	32.23
Fig. 9	163,662	$256 \times 256 \times 128$	10	114.01

**Table 2**  
Accuracy test for our proposed method. Here we use the offset distance  $l = 0.05$  and thickness  $\epsilon = 0.005$ . All tests are performed on the unit cube domain. Here  $\|e^+\|_2$  means the discrete  $l_2$ -norm error of grown surface.

Case	Grid	$\ e^+\ _2$	$\ e^-\ _2$
Cube	$128 \times 128 \times 128$	5.652E-3	6.416E-3
	$256 \times 256 \times 256$	1.565E-3	1.747E-3
Sphere	$128 \times 128 \times 128$	1.804E-3	2.013E-3
	$256 \times 256 \times 256$	4.523E-4	5.243E-4
Cylinder	$128 \times 128 \times 128$	2.264E-3	2.987E-3
	$256 \times 256 \times 256$	5.861E-4	7.581E-4

Fig. 7 shows the reconstruction of Costa–Hoffman–Meeks surface with genus two and engine surfaces. The initial data set is computed by using *Mathematica* software, and the other is taken from [46]. In each row, surface data set, initial reconstruction, and final reconstructed surface are shown. From the initial reconstruction result of engine, we can observe wrinkling surface. However, after eight iterations, we have smooth surface as shown in the last column of Fig. 7.

Fig. 8(a)–(c) show the reconstruction of happy Buddha, bunny, and oil pump surfaces, respectively. From left to right, they are initial data set, final reconstruction, cut and cross views of final offsetting surface, respectively. The initial data sets are taken from [46]. As can be seen, our proposed approach reconstructs the offsetting surface with a uniform distance.

Fig. 9 shows the reconstruction of a skeleton hand on  $\Omega = (0, 2) \times (0, 2) \times (0, 1)$  with a  $256 \times 256 \times 128$  grid. Fig. 9(a)–(c) are the plot of input data set which is taken from [47], isosurfaces of distance function, and final reconstruction, respectively. The computation takes 10 iterations. We can see that our proposed method can handle the complex topology and the reconstructed surface is very smooth compared to the result obtained by using an unsigned distance function.

Next, Table 1 gives the information of the number of data points, the iteration numbers, and the CPU times. The CPU times (seconds) of our calculations, which are performed in C++, are measured on a 3 GHz with 3G of RAM. As can be seen from Table 1, the robustness of our proposed method is observed, as expected from the unconditionally stable discrete schemes.

To test the accuracy of our proposed method, we consider a test with three synthetic surfaces, which are cube, sphere, and cylinder. The side length of cube, the radius of sphere, the radius of cylinder, and the height of cylinder are the same as 0.35. We define the error  $e_m^+ := \mathbf{X}_m^{n,+} - \mathbf{X}_m^{e,+}$ , where  $\mathbf{X}_m^{n,+}$  and  $\mathbf{X}_m^{e,+}$  are numerical and exact grown surface points. Similarly, negative superscript denotes shrunk surface error. See [12] for more details about grown and shrunk surfaces. The errors obtained using these definitions are given in Table 2. Here we use the offset distance  $l = 0.05$  and thickness  $\epsilon = 0.005$ . The numerical results are qualitatively in good agreement with the theoretical values.

In practice, there are outliers or conflicting points into an unorganized point cloud. In Fig. 10(a)–(c), we show offset surface reconstructions with 5%, 10% and 15% random noises. From top to bottom, they are the contour plots of initial shape, the final shape, and plane views in the  $y = 0.5$  with data points. These results suggest that our proposed method can successfully reconstruct the uniform and smooth offset surface. It should be noted that the higher noise level leads to thicker embedding volumes.

#### 4. Conclusion

In this article, we proposed a novel fast and accurate numerical method for the surface embedding narrow volume reconstruction from unorganized points. The method is based on the Allen–Cahn equation with a control function, which restricts the evolution to

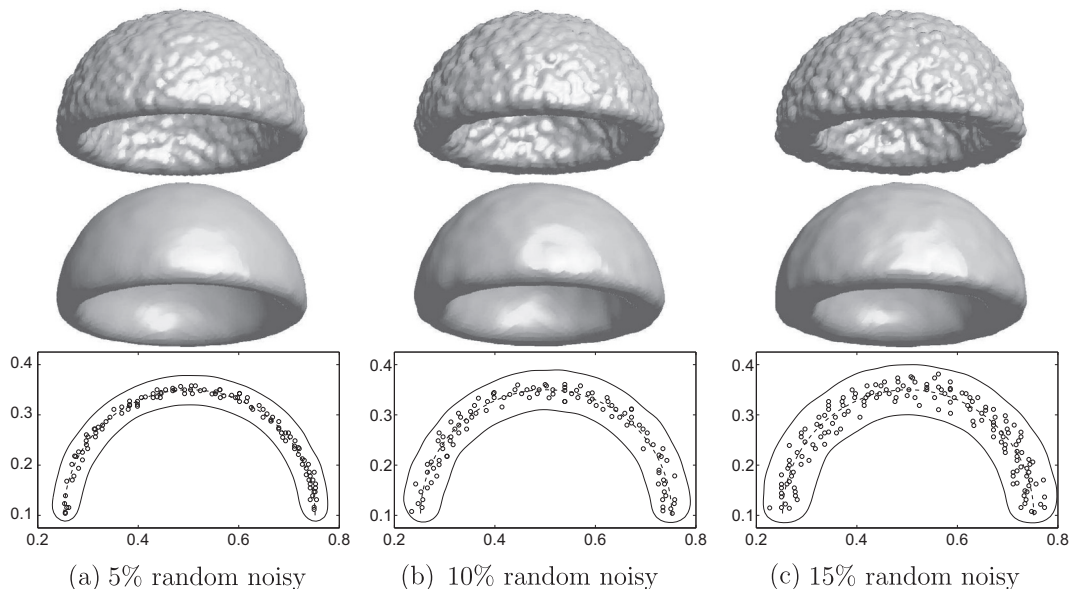


**Fig. 10.** Top row: contour plots of initial shape. Middle row: contour plots of final shape. Bottom row: plane views in the  $y = 0.5$  with data points. Here circle symbols and solid lines denote noises and reconstructed surface, respectively.

the offset regions. The proposed method can deal with non-closed surfaces and do not have self-intersection problems. To overcome the time step restriction, we used an operator splitting technique and proved its unconditional stability. Various numerical experiments were presented to demonstrate the strengths of the proposed method. In future work, to speed up the computation, we will investigate GPU implementation of the current algorithm as done in [22].

## Acknowledgments

The corresponding author (J.S. Kim) was supported by Seoul Science High School R&E program. The second author (D. Lee) was supported by NRF (National Research Foundation of Korea) Grant funded by the Korean Government (NRF-2012-Fostering Core Leaders of the Future Basic Science Program). The authors are grateful to the anonymous referees for their constructive and valuable comments that improved significantly the quality of this paper.

## References

- [1] P. Mancosu, K.F. Jørgensen, S.A. Pedersen, *Visualization, Explanation and Reasoning Styles in Mathematics*, Springer Verlag, 2005.
- [2] F. Bellocchio, N.A. Borghese, S. Ferrari, V. Piuri, *3D Surface Reconstruction*, Springer, New York, 2013.
- [3] R.S. Palais, The visualization of mathematics: towards a mathematical exploratorium, *Notices Am. Math. Soc.* 46 (6) (1999) 647–658.
- [4] Y. Chen, H. Wang, D.W. Rosen, J. Rossignac, Filletting and rounding using a point-based method, in: *DETC05 Proceedings*, 2005.
- [5] T. Tasdizen, R. Whitaker, P. Burchard, S. Osher, Geometric surface processing via normal maps, *ACM Trans. Graph.* 22 (2002) 012–1033.
- [6] R.T. Farouki, The approximation of non-degenerate offset surfaces, *Comput. Aided Geometric Des.* 3 (1986) 15–43.
- [7] J. Klein, G. Zachmann, Point cloud collision detection, in: *Proceedings of EUROGRAPHICS 23*, 2004, pp. 567–76.
- [8] M. Teschner, S. Kimmeler, B. Heidelberger, G. Zachmann, L. Raghupathi, A. Fuhrmann, M.-P. Cani, F. Faure, N. Magnenat-Thalmann, W. Strasser, P. Volino, Collision detection for deformable objects, *Comput. Graph. Forum* 24 (2005) 61–81.
- [9] S. Liu, C.C.L. Wang, Duplex fitting of zero-level and offset surfaces, *Comput.-Aided Des.* 41 (2009) 268–281.
- [10] S. Liu, C.C.L. Wang, Fast intersection-free offset surface generation from freeform models with triangular meshes, *IEEE Trans. Autom. Sci. Eng.* 8 (2011) 347–360.
- [11] C.C.L. Wang, Y. Chen, Thickening freeform surfaces for solid fabrication, *Rapid Prototyping J.* 19 (2013) 395–406.
- [12] Y. Chen, C.C.L. Wang, Uniform offsetting of polygonal model based on layered depth-normal images, *Comput.-Aided Des.* 43 (2011) 31–46.
- [13] B. Curless, M. Levoy, Better optical triangulation through spacetime analysis, in: *Proceedings of IEEE*, 1995, pp. 987–994.
- [14] B. Curless, M. Levoy, A volumetric method for building complex models from range images, in: *Proceedings of SIGGRAPH 96*, 1996, pp. 303–312.
- [15] J.M. Lien, Covering Minkowski sum boundary using points with applications, *Comput. Aided Geom. Des.* 25 (2008) 652–666.
- [16] G. Varadhan, D. Manocha, Accurate Minkowski sum approximation of polyhedral models, in: *Proceedings of 12th Pacific Conference on Computer Graphics and Applications*. *IEEE Comput. Sci.*, 2004, pp. 392–401.
- [17] D. Pavić, L. Kobbelt, High-resolution volumetric computation of offset surfaces with feature preservation, *Comput. Graph. Forum* 27 (2) (2008) 165–174.
- [18] G. Varadhan, S. Krishnan, Y.J. Kim, D. Manocha, Feature-sensitive subdivision and isosurface reconstruction, In: *Proceedings of Visualization 03*, Seattle, 2003, pp. 99–106.
- [19] G. Varadhan, S. Krishnan, D. Manocha, Topology preserving surface extraction using adaptive subdivision, in: *Proceedings of the Symposium Geometry Processing*, 2004, pp. 235–244.
- [20] S.J. Kim, M.Y. Yang, Triangular mesh offset for generalized cutter, *Comput.-Aided Des.* 37 (2005) 999–1014.
- [21] X. Qu, B. Stuycker, A 3D surface offset method for STL-format models, *Rapid Prototyping J.* 9 (2003) 133–141.
- [22] C.C.L. Wang, D. Manocha, GPU-based offset surface computation using point samples, *Comput.-Aided Des.* 45 (2013) 321–330.
- [23] D.E. Breen, S. Mauch, Generating shaded offset surfaces with distance, closest-point and color volumes, in: *Proceedings of the International Workshop on Volume Graphics*, 1999, pp. 307–320.
- [24] D.E. Breen, S. Mauch AUCH, R.T. Whitaker, 3d scan conversion of csg models into distance volumes, in: *Proceedings of the IEEE symposium on Volume visualization*, New York, 1998, pp. 7–14.
- [25] S. Osher, R. Fedkiw, *Level Set Methods and Dynamic Implicit Surfaces*, Springer, 2002.
- [26] C. Colombo, D. Comanducci, A. Del Bimbo, Shape reconstruction and texture sampling by active rectification and virtual view synthesis, *Comput. Vis. Image Underst.* 115 (2011) 161–176.
- [27] Y. Duan, L. Yang, H. Qin, D. Samaras, Shape Reconstruction from 3D and 2D Data Using PDE-Based Deformable Surfaces, *Comput. Vision-ECCV 2004*, 2004, pp. 238–251.
- [28] J.S. Junior, A. Vrabel, O.R.P. Bellon, L. Silva, 3D reconstruction of cultural heritages: challenges and advances on precise mesh integration, *Comput. Vis. Image Underst.* 116 (2012) 1195–1207.
- [29] J. Ye, I. Yanovsky, B. Dong, R. Gandlin, A. Brandt, S. Osher, Multigrid Narrow Band Surface Reconstruction Via Level set Functions, *UCLA CAM reports*, 2009, pp. 09–98.
- [30] H.K. Zhao, S. Osher, R. Fedkiw, Fast surface reconstruction using the level set method, in: *Proceedings of IEEE Workshop on Variational and Level Set Methods in Computer Vision (VLSM)*, 2001.
- [31] H.K. Zhao, S. Osher, B. Merriman, M. Kang, Implicit and nonparametric shape reconstruction from unorganized data using a variational level set method, *Comput. Vis. Image Underst.* 80 (1998) 295–319.
- [32] S.M. Allen, J.W. Cahn, A microscopic theory for antiphase boundary motion and its application to antiphase domain coarsening., *Acta Metall.* 27 (1979) 1085–1095.
- [33] M. Beneš, V. Chaloupecký, K. Mikula, Geometrical image segmentation by the Allen–Cahn equation, *Appl. Numer. Math.* 51 (2004) 187–205.
- [34] J.A. Dobrosotskaya, A.L. Bertozzi, A Wavelet–Laplace variational technique for image deconvolution and inpainting, *IEEE Trans. Image Process.* 17 (2008) 657–663.
- [35] C. Samson, L. Blanc-Fraud, G. Aubert, J. Zerubia, A variational model for image classification and restoration, *IEEE Trans. Pattern Anal. Mach. Intell.* 22 (2000) 460–472.
- [36] J. Lie, M. Lysaker, X.-C. Tai, A binary level set model and some applications to Mumford–Shah image segmentation, *IEEE. Trans. Image Process.* 15 (2006) 1171–1181.
- [37] Y. Li, J. Kim, An unconditionally stable numerical method for bimodal image segmentation, *Appl. Math. Comput.* 219 (2012) 3083–3090.
- [38] Y. Li, J. Kim, Multiphase image segmentation using a phase-field model, *Comput. Math. Appl.* 62 (2011) 737–745.
- [39] Y. Li, J. Kim, A fast and accurate numerical method for medical image segmentation, *J. KSIAM* 14 (2010) 201–210.
- [40] Y. Li, H.-G. Lee, D. Jeong, J. Kim, An unconditionally stable hybrid numerical method for solving the Allen–Cahn equation, *Comput. Math. Appl.* 60 (6) (2010) 1591–1606.
- [41] U. Trottenberg, C. Oosterlee, A. Schüller, *Multigrid*, Academic Press, USA, 2001.
- [42] W.E. Boyce, R.C. DiPrima, *Elementary Differential Equations and Boundary Value Problems*, tenth ed., Wiley, USA, 2012.
- [43] V.S. Ryaben'kii, S.V. Tsynkov, *A Theoretical Introduction to Numerical Analysis*, Chapman and Hall/CRC Press, Boca Raton, 2007.
- [44] K.W. Morton, D.E. Mayers, *Numerical Solution of Partial Differential Equations*, Cambridge University Press, Cambridge, UK, 1996.
- [45] J. Kim, Phase-field models for multi-component fluid flows, *Commun. Comput. Phys.* 12 (2012) 613–661.
- [46] <http://research.microsoft.com/en-us/um/people/hoppe>.
- [47] [http://www.cc.gatech.edu/projects/large\\_models](http://www.cc.gatech.edu/projects/large_models).